JAAS

Dynamic Article Links

Cite this: *J. Anal. At. Spectrom.*, 2012, **27**, 479

www.rsc.org/jaas

PAPER

Precise micrometre-sized Pb-Pb and U-Pb dating with NanoSIMS

Wei Yang,*[a] Yang-Ting Lin,[b] Jian-Chao Zhang,[b] Jia-Long Hao,[b] Wen-Jie Shen[b] and Sen Hu[b]

Received 10th October 2011, Accepted 19th January 2012
DOI: 10.1039/c2ja10303f

We report a new method of Pb-Pb dating for zircon and baddeleyite with a lateral resolution of <2 μm and U-Pb dating for zircon with a lateral resolution of <5 μm using CAMECA NanoSIMS 50L. The O^- primary beam was optimized to a current of ~500 pA with a diameter of 1.7 μm. The zircon standard M257 and baddeleyite standard Phalaborwa were dated by the Pb-Pb method, yielding $^{207}Pb/^{206}Pb$ ages of 563 ± 14 Ma and 2058 ± 6 Ma, respectively. These results agree well with the recommended ages within analytical uncertainties. Four zircon standards, including Qinghu, Plesovice, Temora, and 91500 were dated by the U-Pb method. The samples were measured in a scanning mode by rastering 3 × 3 μm^2 areas in order to eliminate pit depth-dependent U-Pb fractionation. The weighted average $^{206}Pb/^{238}U$ ages obtained by this method for the four zircon standards are 158 ± 3 Ma, 337 ± 7 Ma, 427 ± 10 Ma, and 1076 ± 14 Ma, respectively. These results are consistent with the reported ID-TIMS ages of these samples within error. Our study demonstrates that Pb-Pb ages of zircon and baddeleyite can be determined with a lateral resolution of <2 μm, and U-Pb ages of zircon can be measured with a lateral resolution of <5 μm by CAMECA NanoSIMS. This technique will have important applications to high lateral resolution dating, such as thin layers of zoned zircons, small grains of lunar zircon, and micron-sized baddeleyites in Martian meteorites and in various achondrites from differentiated asteroids.

1. Introduction

Zircon ($ZrSiO_4$) is a common accessory mineral occurring in a wide variety of terrestrial and extraterrestrial rocks.[1] Because it is highly enriched in U and strongly depleted in the daughter element Pb during crystal growth, zircon U-Pb dating has become the most commonly used geochronometer.[2] The potential applications of secondary ion mass spectrometry (SIMS) for U-Pb geochronology was first demonstrated by Andersen and Hinthorne.[3] The Sensitive High-Resolution Ion Micro-Probe (SHRIMP) then opened up a new chapter in zircon geochronology.[4,5] Nowadays, SHRIMP and CAMECA ims-1270/1280 are used routinely for U-Pb geochronology, which can determine U-Pb zircon ages with a precision of *ca.* 1% and a lateral resolution of *ca.* 20–30 μm.[6]

There are increasing requirements for a high lateral resolution (*e.g.*, <5 μm) of U-Pb and Pb-Pb geochronology for dating small but precious zircon samples. Many zircons are fine-grained and/or have complex structures and chemical zoning features such as those from ultra-high pressure metamorphosed rocks[7] and from heavily shocked lunar rocks.[8,9] Furthermore, other minerals such as baddeleyite are also widely used for U-Pb geochronological dating. However, only micron-sized baddeleyites are available in some cases such as those in Martian meteorites and differentiated asteroids.

U-Pb zircon dating at a scale of <5 μm was recently carried out using CAMECA ims-1280 with a precision of 1–2%.[10] One of the technique challenges of this method is to achieve a high intensity primary beam with a few micron diameters. The authors optimized a Gaussian distribution primary O_2^- probe of ~100 pA in a diameter of ~5 μm.

In comparison with ims-1280, CAMECA NanoSIMS, which is designed for high lateral resolution applications, can operate with a very high density primary beam (*e.g.*, 4 nA in a diameter of ~5 μm).[11] A few U-Pb and Pb-Pb measurements with NanoSIMS have been reported. Stern *et al.*[12] obtained a $^{207}Pb/^{206}Pb$ age of 504 ± 18 Ma for zirconolite ($CaZrTi_2O_7$) using a primary O^- beam of ~100 pA and ~4.5 μm diameter. However, the precision is relatively poor and Pb/U was not measured so there was no test for concordance. Sano *et al.*[11] reported ^{238}U-^{206}Pb and ^{207}Pb-^{206}Pb dating methods of monazite using a ~4 nA O^- primary beam with a diameter of 5–7 μm. Takahata *et al.*[13] applied similar method to zircon using a larger and higher intensity O^- probe (~9 nA and 15 μm). These methods have achieved U-Pb age precision of 1 ~ 2%, however, their lateral resolutions are at a scale of 5–15 μm, limiting the applications for small sample dating analyses.

Here we present a new method using the NanoSIMS 50L to conduct zircon Pb-Pb isotope dating at a scale <2 μm and U-Pb isotope dating at a scale <5 μm. A ~500 pA O^- primary beam with a diameter of 1.7 μm was obtained by optimizing the primary column, and brightness of the probe is higher than those

[a]*State Key Laboratory of Lithospheric Evolution, Institute of Geology and Geophysics, Chinese Academy of Sciences, Beijing, 100029, China. E-mail: yangw@mail.iggcas.ac.cn; Fax: +86 10 62010846; Tel: +86 10 82998514*
[b]*Key Laboratory of the Earth's Deep Interior, Institute of Geology and Geophysics, Chinese Academy of Sciences, Beijing, 100029, China*

achieved for U-Pb dating by a factor >2. As demonstrated by this method, Pb-Pb ages of zircon and baddeleyite can be determined with a lateral resolution of <2 μm, and U-Pb ages of zircon can be measured with a lateral resolution of <5 μm.

2. Standard samples

Several standard samples, including one glass (NIST610), five zircon standards (M257, 91500, Plesovice, Qinghu, Temorra) and one baddeleyite standard (Phalaborwa) were embedded in epoxy and well polished. These standard samples have been analyzed for Pb-Pb and U-Pb dating methods by Thermal Ionization Mass Spectrometry (TIMS).[14–20] A brief description of these samples is provided below in Table 1.

The NIST610 glass is a silicate glass reference material produced by the National Institute of Standards and Technology (NIST). It contains U of 513.3 ± 0.9 ppm and Pb of 389.0 ± 7.0 ppm[21] with TIMS-determined $^{206}Pb/^{204}Pb$ ratio of 17.047 ± 0.0018 and $^{207}Pb/^{204}Pb$ ratio of 15.509 ± 0.0010.[22]

The Qinghu zircon was separated from a felsic syenite rock at a large quarry in the Qinghu Provinces of South China. It has concordant U-Pb ages (with $^{206}Pb/^{238}U$ age of 159.5 ± 0.2 Ma dated by ID-TIMS) and homogeneous hafnium and oxygen isotopes.[14] The Plesovice zircon comes from a granulite facies potassic rock at the Plesovice quarry in the southern Bohemian Massif, Czech Republic. It is concordant in the U-Pb isotopic system, with a weighted mean $^{206}Pb/^{238}U$ age of 337.1 ± 0.4 Ma dated by ID-TIMS.[15] The Temora zircon was derived from the Middledale Gabbroic Diorite, a high-level mafic stock within the Palaeozoic Lachlan Orogen of eastern Australia. Its $^{206}Pb/^{238}U$ ID-TIMS age has been determined to be 416.8 ± 0.3 Ma.[16] The M257 zircon was an oval shaped, cut stone originated from the Ratnapura district, Sri Lanka. It has TIMS-determined $^{206}Pb/^{238}U$ ratio of 0.09100 ± 0.00003 (2σ) and $^{207}Pb/^{235}U$ ratio of 0.7392 ± 0.0003, corresponding to 561.3 ± 0.3 Ma.[17] The 91500 zircon is a fragment of a single crystal from Kuehl Lake, Ontario, Canada. It gave a mean $^{207}Pb/^{206}Pb$ age of 1062.4 ± 0.8 Ma and a $^{206}Pb/^{238}U$ age of 1065.4 ± 0.6 Ma by TIMS.[18]

The Phalaborwa baddeleyite came from a large crystal obtained from the Phalaborwa carbonatite, South Africa, which yielded a mean $^{207}Pb/^{206}Pb$ age of 2059.6 ± 0.4 Ma.[19,20]

3. Instrument and method

3.1. Instrument

The Pb-Pb and U-Pb analyses were carried out using a CAMECA NanoSIMS 50L at the Institute of Geology and Geophysics, Chinese Academy of Sciences (IGGCAS). NanoSIMS is a scanning ion microprobe possessing a double-focusing mass analyzer capable of high mass and lateral resolution.[23] One of the major advantages of NanoSIMS over other conventional SIMS is the coaxial design, which includes a normal primary ion incidence and a co-axial secondary ion extraction to optimize simultaneously objective lens performance and ion collection. This design allows to reduce the objective-sample distance (0.4 mm), leading to very low aberration coefficients and thus to a smaller spot size for a given probe current than other conventional SIMS.[23]

Table 1 Reference materials used in this study

Sample Name	Matrix	Recommended values
NIST610	Glass	$^{206}Pb/^{204}Pb = 17.047 \pm 0.002$, $^{207}Pb/^{204}Pb = 15.509 \pm 0.001$
Qinghu	Zircon	$^{206}Pb/^{238}U$ age = 159.5 ± 0.2 Ma
Plesovice	Zircon	$^{206}Pb/^{238}U$ age = 337.1 ± 0.4 Ma
Temora	Zircon	$^{206}Pb/^{238}U$ age = 416.8 ± 0.3 Ma
M257	Zircon	$^{206}Pb/^{238}U$ age = 561.3 ± 0.3 Ma
91500	Zircon	$^{206}Pb/^{238}U$ age = 1065.4 ± 0.6 Ma
Phalaborwa	Baddeleyite	$^{207}Pb/^{206}Pb$ age = 2059.6 ± 0.4 Ma

3.2. Oxygen probe

The primary column of the NanoSIMS incorporates a duo plasmatron ion source in which the negative oxygen ions pass through a Wien velocity filter (for isolation of $^{16}O^-$), and are focused to the target surface with a total impact energy of 16 keV. A high density of O^- beam (~500 pA) was optimized with the following configuration of the apertures (D0-3 = 100 μm, D1-2 = 300 μm) and lens (L0 = ~5.6 kV, L1 = ~5.1 kV). In order to minimize the size of probe, it was then focused with the EOP, and the astigmatic aberration was eliminated with the octupole stigmators (Oct-45 and Oct-90), by rastering a 40 × 40 μm^2 area on an Al–Cu grid (Fig. 1a).

The primary ion beam results in an approximately Gaussian density distribution at the target surface (*i.e.*, critical illumination). Lateral resolution can be determined with the knife-edge method, *i.e.*, the linear distance between the 16 and 84% relative intensity of $^{27}Al_2^+$ signals measured across the boundary of the Al-Cu grid. The diameter of the primary O^- beam was ~1.7 μm as measured by this method (Fig. 1b). The beam density is about 22 mA cm^{-2}, similar to those obtained by other NanoSIMS (*e.g.*, 4 nA, 5 μm, 20 mA cm^{-2}),[11] and significantly higher than the probe of CAMECA ims-1280 (*e.g.*, 100 pA, 5 μm, 0.5 mA cm^{-2}).[10]

3.3. Mass analyzer

The secondary ions were extracted from the sample surface by the co-axial immersion lens, and focused onto a fixed-width analyzer entrance slit (ES). Less than 50% of secondary ion was cut with ES-3 (relative to full transmission without slits), about 10% at the aperture slit (AS-1), and 10% at the high energy slit (EnS) that is used to reduce chromatic aberration. Accordingly, the relative transmission at high resolution was ~30%. The sensitivity for Pb^+ under these conditions was 4 cps/ppm/nA, similar to the Pb^+ sensitivity reported by Stern *et al.*[12] and Sano *et al.*,[11] but substantially lower than that of CAMECA ims-1280 with oxygen flooding technique.[10]

There are 7 detectors in the NanoSIMS 50L, which permit up to 7 secondary ion species to be simultaneously counted. With a Mattauch-Herzog geometry, the multi-collector system can cover a wide mass range. Therefore, it is possible to detect ^{206}Pb, ^{238}U, and $^{238}U^{16}O_2$ simultaneously. However, it is impossible to count ^{204}Pb and ^{206}Pb or ^{207}Pb at the same time because the dispersion distance between ^{204}Pb and ^{206}Pb or ^{207}Pb at the focal plane is too short to place more than one detector. Therefore, magnetic peak-switching mode was applied for Pb-Pb dating.

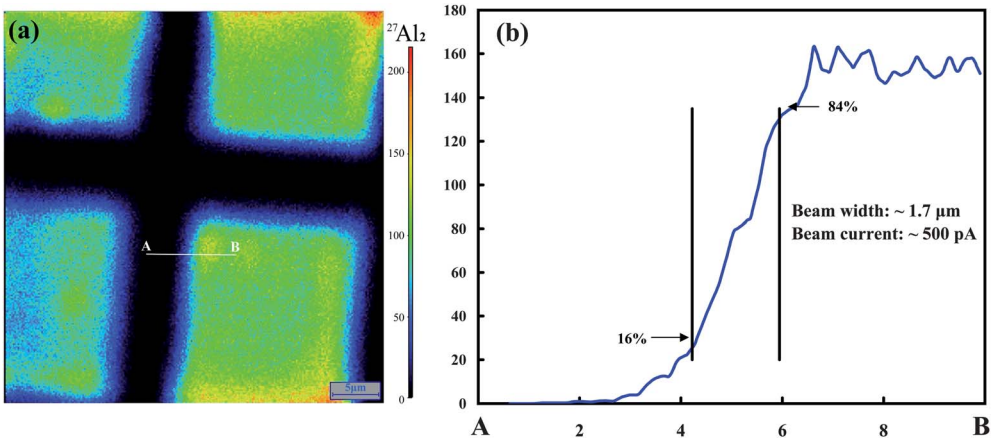

Fig. 1 (a) Real Time Image (ROI) of $^{27}Al_2^+$ obtained by sputtering a 40 × 40 µm² area on Al–Cu grid with O^- primary ion beam. (b) ^{27}Al intensity along the profile AB. The measured beam width of the ~500 pA primary beam by knife-edge method is ~1.7 µm.

The magnetic field was switched to measure background (203.5), ^{204}Pb, ^{206}Pb and ^{207}Pb in an up-mass sequence (Table 2). On the other hand, combined analysis mode was used for U-Pb dating. At this mode, the species $^{90}Zr_2{}^{16}O$, ^{238}U, $^{238}U^{16}O$ and $^{238}U^{16}O_2$ were simultaneously measured with ^{206}Pb when the magnetic field rests on B3 (Table 2).

The mass calibration was carried out alternatively by using NIST 610 glass and M257 zircon standard. Mass peak of ^{204}Pb

Table 2 Pb-Pb and U-Pb dating method by using NanoSIMS

	Pb-Pb analysis	U-Pb analysis				
Magnetic field	EM#2	EM#1	EM#2	EM#3	EM#4	EM#5
B1	203.5(background)		203.5			
B2	204(^{204}Pb)		204(^{204}Pb)			
B3	206(^{206}Pb)	196(Zr_2O)	206(^{206}Pb)	238(U)	254(UO)	270(UO_2)
B4	207(^{207}Pb)		207(^{207}Pb)			

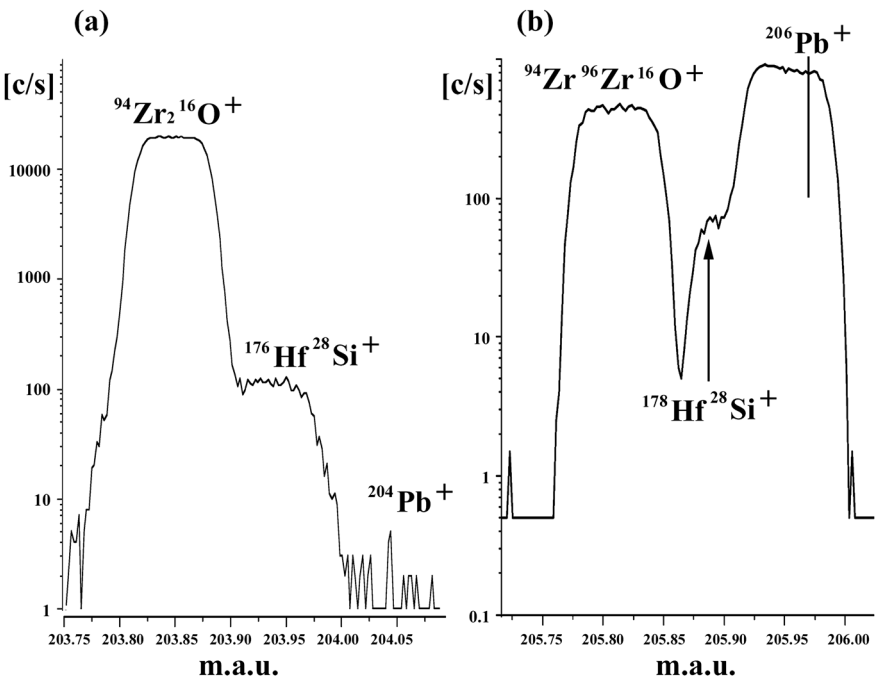

Fig. 2 Mass spectrum in the vicinity of $m/z = 204$ (a) and 206 (b) in the standard zircon M257. Mass resolution for $^{206}Pb = 5000$ at 10% peak height. ^{206}Pb is well separated from $^{94}Zr^{96}Zr^{16}O$ with adequate flat-topped peak. The vertical line at ^{206}Pb peak represents the counting position. Tail of $^{178}Hf^{28}Si$ is as expected insignificant at ^{206}Pb.

was centred with NIST610, while the other peaks were centred with M257. A mass resolution of 5000 at 10% peak height was obtained to separate ^{206}Pb from the interference $^{178}Hf^{28}Si$ with adequate flat topped peaks (Fig. 2).

3.4. The effect of crater depth on U-Pb fractionation

There are two sputtering modes (static and scanning) of primary ion beam on the target surface. The former (scanning off mode) sputters a spot, whereas the latter (scanning on mode) scans an area. In the scanning off mode, the impact pits are the smallest, about the diameter of the probe (1.7 μm). However, large depth-dependent U-Pb fractionation was observed at this mode. For example, when sputtering a spot at the scanning off mode, the sensitivities of ^{238}U (Fig. 3a), $^{238}U^{16}O$ and $^{238}U^{16}O_2$ (not shown here) increased significantly with time. Hence, it is hard to determine their count rates with high precisions (*e.g.* <1%). By contrast, the sensitivities of ^{238}U (Fig. 3b), $^{238}U^{16}O$ and $^{238}U^{16}O_2$ (not shown here) kept constant when sputtering an area of 10 × 10 μm^2 for a period up to 30 min.

This large U-Pb fractionation at the scanning off mode may be derived from the shape of the craters. Because of the Gaussian density distribution of the primary ion beam, the crater developed on the sample target is V-shaped when turning off the scanning mode (Fig. 4a, b). This V-shaped crater may influence the sputter yield because the angle of incidence changes.[24] By contrast, when an area is sputtered at the scanning on mode, the crater can preserve a relatively flat bottom (*e.g.*, 3 × 3 μm^2; Fig. 4c, d). U-Pb fractionation with sputtering time can be eliminated. To achieve lateral resolution as high as possible and limit U-Pb fractionation with crater development, a series of rastering areas have been tested. The results show that when turning on scanning mode to sputter an area of 3 × 3 μm^2, the U-Pb fractionation is acceptably limited (1SD of $^{206}Pb/^{238}U$ for 300 measurements on M257 zircon in 30 min <2%) (Fig. 3c). The lateral resolution for this U-Pb measurement is about 4.7 μm.

Notably, the sensitivity of Pb always kept stable (1SD of 300 measurements on M257 zircon in 30 min <3%) at both scanning on and off mode, indicating that the influence of Pb sensitivity by V-shape crater development is very limited. The reason is still unknown and more investigations are required to address the mechanism in the future. Nevertheless, this observation makes it possible to measure Pb isotopes precisely at scanning off mode. Thus, the lateral resolution for Pb-Pb measurement by turning off scanning can be at a scale of 1.7 μm.

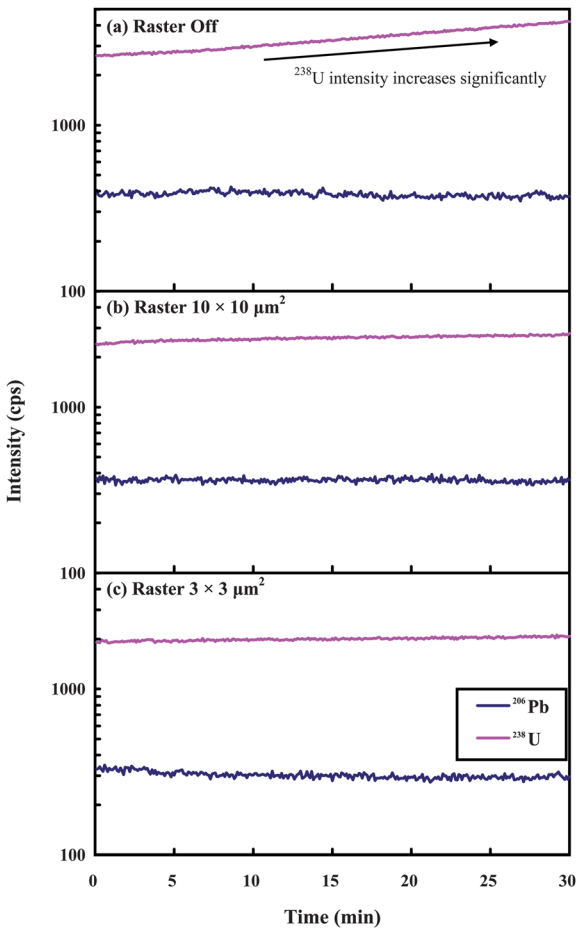

Fig. 3 Intensity variations of ^{206}Pb and ^{238}U for 30 min by three raster modes: (a) scanning mode off, (b) scanning mode on and rastering of a 10 × 10 μm^2 area, (c) scanning mode on and rastering a 3 × 3 μm^2 area. ^{238}U intensity increases significantly under scanning mode off, indicating large U-Pb fractionation driven by "V-shaped" crater development.

3.5. Data acquisition

Before counting, the sample surface was rastered by 6 × 6 μm^2 for 3 min in order to remove surface contaminant of common Pb. For Pb-Pb analyses, the magnetic field was cyclically peak-stepped through a series of mass numbers 203.5 (background), 204 (^{204}Pb), 206 (^{206}Pb), and 207 (^{207}Pb). All signals were counted by the same electron multiplier (here EM#2). The scanning off

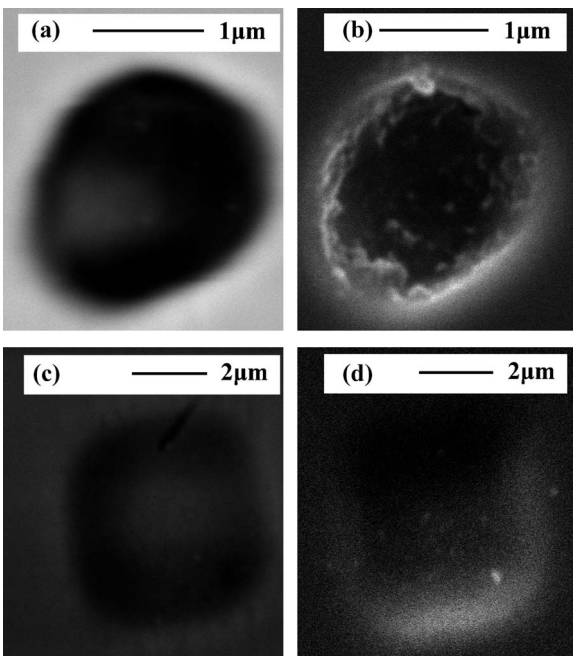

Fig. 4 The backscatter (a, c) and secondary electron (b, d) images of the O^- beam crater on zircon sputtered for ~30 min. (a)(b): scanning off mode for Pb-Pb dating; (c)(d): scanning on mode (3 × 3 μm^2) for U-Pb dating.

mode was used, and the total analysis time was about 30 min. For U-Pb analyses, the primary ion beam rastered a 3×3 μm^2 area. The magnetic field was also cyclically peak-stepped through mass numbers of 203.5 (background), 204 (^{204}Pb), 206 (^{206}Pb), and 207 (^{207}Pb) for about 30 min. Other ion species of $^{90}Zr_2{}^{16}O$, ^{238}U, $^{238}U^{16}O$ and $^{238}U^{16}O_2$ were simultaneously measured with ^{206}Pb (Table 2). Uncertainties of individual analyses in Table 3 and 4 are reported at a 1σ level. Mean ages are quoted with 95% confidence interval by pooling multiple U-Pb and Pb-Pb analyses of the same samples. Measured ^{204}Pb/^{206}Pb ratios were used for the correction of common Pb, whose isotopic compositions were assumed by a two-stage evolution model.[25] Isoplot program[26] was used for data processing and age calculation.

4. Results and discussion

4.1. Instrumental mass fractionation (IMF)

The mass fractionation of Pb isotopes and the isobaric interference of Pb hydrides are two main challenges for accurate Pb

Table 3 Pb isotopic data of NIST610 glass and M257 zircon obtained by NanoSIMS

Spot No.	^{204}Pb/^{206}Pb	± (1σ)	^{207}Pb/^{206}Pb	± (1σ)	^{207}Pb*/^{206}Pb*	± (1σ)
Nist610_1	0.0609	0.0010	0.915	0.007		
Nist610_2	0.0588	0.0009	0.922	0.006		
Nist610_3	0.0598	0.0011	0.916	0.010		
Nist610_4	0.0596	0.0012	0.916	0.006		
Nist610_5	0.0581	0.0010	0.907	0.007		
Nist610_6	0.0584	0.0012	0.912	0.007		
Nist610_7	0.0588	0.0010	0.909	0.007		
Nist610_8	0.0586	0.0010	0.921	0.007		
Nist610_9	0.0592	0.0011	0.902	0.007		
Nist610_10	0.0616	0.0013	0.908	0.007		
M257_1	0.000086	0.000027	0.0598	0.0010	0.0585	0.0011
M257_2	0.000045	0.000027	0.0585	0.0008	0.0579	0.0009
M257_3	0.000072	0.000017	0.0601	0.0009	0.0590	0.0009
M257_4	0.000068	0.000020	0.0589	0.0011	0.0579	0.0011
M257_5	0.000065	0.000020	0.0589	0.0012	0.0580	0.0013
M257_6	0.000064	0.000017	0.0602	0.0010	0.0592	0.0011
M257_7	0.000061	0.000009	0.0588	0.0008	0.0579	0.0008
M257_8	0.000076	0.000022	0.0608	0.0015	0.0597	0.0015
M257_9	0.000050	0.000011	0.0605	0.0013	0.0597	0.0013
M257_10	0.000047	0.000008	0.0584	0.0015	0.0577	0.0015
M257_11	0.000059	0.000025	0.0603	0.0022	0.0595	0.0022
M257_12	0.000032	0.000016	0.0594	0.0007	0.0589	0.0008
M257_13	0.000042	0.000017	0.0607	0.0008	0.0601	0.0008
M257_14	0.000051	0.000015	0.0584	0.0007	0.0576	0.0007
M257_15	0.000031	0.000014	0.0607	0.0013	0.0603	0.0013
M257_16	0.000033	0.000010	0.0596	0.0006	0.0591	0.0006
M257_17	0.000033	0.000010	0.0592	0.0009	0.0587	0.0009
M257_18	0.000030	0.000009	0.0600	0.0008	0.0595	0.0008
M257_19	0.000033	0.000011	0.0598	0.0007	0.0593	0.0007
M257_20	0.000035	0.000010	0.0603	0.0014	0.0598	0.0014
M257_21	0.000033	0.000012	0.0605	0.0016	0.0600	0.0016
M257_22	0.000078	0.000033	0.0600	0.0011	0.0589	0.0012
M257_23	0.000043	0.000021	0.0586	0.0013	0.0580	0.0014
M257_24	0.000088	0.000050	0.0609	0.0011	0.0596	0.0013
M257_25	0.000065	0.000025	0.0589	0.0017	0.0580	0.0017
M257_26	0.000047	0.000028	0.0599	0.0012	0.0592	0.0013
M257_27	0.000062	0.000053	0.0583	0.0015	0.0574	0.0017
M257_28	0.000089	0.000076	0.0594	0.0013	0.0581	0.0017
Pha_1	0.000022	0.000003	0.1263	0.0010	0.1260	0.0010
Pha_2	0.000018	0.000003	0.1287	0.0006	0.1284	0.0006
Pha_3	0.000018	0.000004	0.1267	0.0010	0.1264	0.0010
Pha_4	0.000014	0.000002	0.1274	0.0008	0.1272	0.0008
Pha_5	0.000010	0.000002	0.1262	0.0008	0.1260	0.0008
Pha_6	0.000017	0.000004	0.1279	0.0011	0.1277	0.0011
Pha_7	0.000080	0.000021	0.1268	0.0008	0.1257	0.0008
Pha_8	0.000014	0.000003	0.1265	0.0011	0.1263	0.0011
Pha_9	0.000083	0.000022	0.1284	0.0007	0.1272	0.0008
Pha_10	0.000093	0.000029	0.1277	0.0010	0.1265	0.0011
Pha_11	0.000032	0.000005	0.1269	0.0007	0.1265	0.0007
Pha_12	0.000030	0.000005	0.1298	0.0013	0.1294	0.0013
Pha_13	0.000014	0.000003	0.1276	0.0009	0.1274	0.0009
Pha_14	0.000011	0.000003	0.1276	0.0008	0.1274	0.0008
Pha_15	0.000019	0.000005	0.1273	0.0010	0.1271	0.0011
Pha_16	0.000010	0.000003	0.1272	0.0008	0.1271	0.0008
Pha_17	0.000026	0.000006	0.1274	0.0013	0.1270	0.0013
Pha_18	0.000011	0.000004	0.1268	0.0010	0.1266	0.0010

Table 4 U-Pb dating results of standard zircons (Qinghu, Plesovice, Temora, 91500) by using NanoSIMS

	Isotopic ratios						Age (Ma)					
Spot No.	$^{207}Pb/^{206}Pb$	1σ %	$^{207}Pb/^{235}U$	1σ %	$^{206}Pb/^{238}U$	1σ %	$^{207}Pb/^{206}Pb$	1σ	$^{207}Pb/^{235}U$	1σ	$^{206}Pb/^{238}U$	1σ
QH_1	0.0504	8.3	0.174	8.8	0.0250	3.0	211.5	180.7	162.8	13.3	159.4	4.7
QH_2	0.0516	6.6	0.177	7.3	0.0249	3.0	265.6	145.4	165.7	11.2	158.8	4.7
QH_3	0.0509	6.1	0.176	7.0	0.0251	3.5	237.7	134.7	164.9	10.7	159.9	5.5
QH_4	0.0485	8.9	0.169	9.5	0.0253	3.2	124.7	198.0	158.9	14.0	161.3	5.0
QH_5	0.0540	9.2	0.184	10.0	0.0247	4.1	369.7	193.9	171.4	15.9	157.3	6.3
QH_6	0.0520	8.3	0.178	9.2	0.0249	4.0	284.0	179.1	166.7	14.2	158.5	6.2
QH_7	0.0518	5.0	0.174	5.8	0.0244	3.0	274.4	109.6	162.9	8.7	155.4	4.5
QH_8	0.0700	18.9	0.235	20.1	0.0243	7.0	929.5	346.2	214.0	39.6	154.7	10.7
QH_9	0.0513	16.4	0.184	17.2	0.0260	4.9	253.5	339.7	171.2	27.4	165.3	8.0
QH_10	0.0523	8.3	0.175	9.7	0.0242	5.0	299.6	178.6	163.5	14.8	154.3	7.7
QH_11	0.0497	8.3	0.162	10.0	0.0237	5.5	182.3	183.5	152.8	14.3	150.9	8.2
QH_12	0.0572	18.1	0.200	18.7	0.0253	4.8	498.0	355.0	184.7	32.1	161.2	7.6
QH_13	0.0512	10.8	0.172	11.7	0.0244	4.6	248.5	231.2	161.4	17.7	155.5	7.1
QH_14	0.0515	15.5	0.176	16.8	0.0248	6.6	262.7	321.7	164.7	25.9	158.0	10.3
QH_15	0.0524	12.2	0.178	13.1	0.0246	4.5	302.1	257.3	166.0	20.2	156.7	7.0
Ple_1	0.0590	8.2	0.436	8.6	0.0536	2.6	566.7	169.0	367.5	26.8	336.7	8.5
Ple_2	0.0545	8.6	0.415	9.1	0.0552	3.0	393.4	182.4	352.3	27.5	346.1	10.1
Ple_3	0.0561	6.8	0.406	7.1	0.0526	2.0	456.1	145.0	346.3	21.1	330.2	6.3
Ple_4	0.0570	6.8	0.429	7.9	0.0546	4.0	491.7	142.9	362.8	24.4	342.9	13.5
Ple_5	0.0549	7.4	0.418	7.8	0.0552	2.6	409.3	157.1	354.4	23.7	346.1	8.9
Ple_6	0.0564	8.2	0.409	8.9	0.0526	3.5	467.4	171.8	348.3	26.6	330.6	11.3
Ple_7	0.0517	11.2	0.388	12.0	0.0544	4.2	271.9	238.6	332.9	34.5	341.7	13.8
Tem_1	0.0594	8.7	0.570	9.2	0.0696	3.0	582.7	179.1	458.1	34.6	433.6	12.4
Tem_2	0.0600	7.4	0.576	8.1	0.0697	3.3	602.7	152.7	461.9	30.6	434.1	13.8
Tem_3	0.0640	14.3	0.615	14.7	0.0696	3.7	742.7	275.6	486.5	58.6	433.9	15.7
Tem_4	0.0597	13.5	0.572	14.2	0.0695	4.2	591.2	269.1	459.4	53.7	433.4	17.6
Tem_5	0.0600	10.0	0.577	12.0	0.0698	6.6	602.0	203.2	462.7	45.6	435.1	27.8
Tem_6	0.0601	8.7	0.574	10.0	0.0693	4.9	605.6	178.4	460.6	37.8	432.1	20.6
Tem_7	0.0623	19.1	0.588	20.0	0.0685	5.8	683.6	362.7	469.7	78.0	427.1	23.9
Tem_8	0.0606	15.8	0.578	16.3	0.0692	3.8	624.3	308.6	463.3	62.3	431.5	15.8
Tem_9	0.0612	14.8	0.586	15.1	0.0694	3.0	647.1	289.4	468.5	58.2	432.8	12.4
Tem_10	0.0606	17.0	0.583	17.3	0.0697	3.0	626.5	329.6	466.1	66.7	434.2	12.7
Tem_11	0.0634	25.4	0.591	25.9	0.0675	5.1	723.3	463.1	471.5	102.8	421.4	20.8
Tem_12	0.0670	12.0	0.603	13.2	0.0652	5.5	838.8	232.3	478.9	51.8	407.2	21.8
Tem_13	0.0657	16.5	0.581	17.1	0.0642	4.6	795.9	313.0	465.1	66.1	400.9	17.8
Tem_14	0.0704	17.3	0.648	18.0	0.0667	5.0	941.4	318.8	507.2	74.4	416.3	20.0
Tem_15	0.0691	24.9	0.649	25.8	0.0681	7.0	903.1	442.8	508.0	108.9	424.7	28.8
91500_1	0.0766	10.6	1.922	10.7	0.1820	1.6	1110.3	197.6	1088.7	74.0	1078.0	16.1
91500_2	0.0734	11.2	1.848	11.3	0.1825	1.5	1025.9	210.7	1062.7	77.1	1080.6	15.2
91500_3	0.0807	10.5	1.993	10.7	0.1792	2.0	1213.1	194.3	1113.0	75.1	1062.6	19.2
91500_4	0.0776	11.9	1.929	12.0	0.1802	1.5	1137.3	220.3	1091.0	83.6	1068.0	14.8
91500_5	0.0745	10.4	1.876	10.6	0.1826	1.9	1055.0	196.6	1072.5	72.6	1081.2	18.8
91500_6	0.0779	10.7	1.988	10.9	0.1851	2.3	1144.5	198.8	1111.5	76.6	1094.7	23.1
91500_7	0.0769	12.0	1.947	12.7	0.1836	4.2	1118.7	222.5	1097.5	89.2	1086.9	42.6

isotopic measurements using SIMS. However, their influences are negligible for mono-collector SIMS Pb isotope measurements, as there appears to be a mutual cancellation of each other.[6] Previous studies with NanoSIMS have demonstrated that the instrumental mass fractionation (IMF) of Pb isotopes can be neglected by using magnet peak switching (one collector) mode. For example, the Pb isotopic measurements of SRM Pb metals, zirconolite[12] and NIST610 glass[11] by NanoSIMS show negligible IMF values. The contribution of hydride and the total IMF values with NanoSIMS in this study will be discussed below.

Since it is impossible to obtain a high enough mass resolution of >30 000 to separate PbH isobars, The contribution of hydride and its influence on $^{207}Pb/^{206}Pb$ ratio were evaluated by measuring $^{208}PbH/^{208}Pb$ ratio. The ^{208}PbH signal on zircon can not be detected with current O^- primary beam of ~500 pA, Thus, a natural galena (PbS) was measured. Ten measurements gave a weighted average $^{208}PbH/^{208}Pb$ ratio of 0.0000525 ± 0.0000012 (2σ) (Fig. 5). For zircons older than 100 Ma, because their $^{207}Pb/^{206}Pb$ ratios are larger than 0.048, the contribution from ^{206}PbH to ^{207}Pb is less than 0.2% and can be negligible.

In addition, the total IMF values were analyzed using NIST610 glass. In general, the instrumental mass fractionation (IMF) of Pb is reported as deviations in % per atomic mass unit from the reference material. $IMF = 100 \times (R_m/R_s - 1)/(M_2 - M_1)$, where M_1 and M_2 are nominal masses, R_m is the measured ratio (M_2/M_1), and R_s is the ratio of the reference material.

The Pb-Pb isotopic ratios of NIST610 glass are presented in Table 3 and plotted in Fig. 6. Ten measurements yield a weighted average $^{204}Pb/^{206}Pb$ ratio of 0.05929 ± 0.00067 (2σ) and a weighted average $^{207}Pb/^{206}Pb$ ratio of 0.9131 ± 0.0043 (2σ). The mean IMF values calculated for $^{204}Pb/^{206}Pb$ and $^{207}Pb/^{206}Pb$ ratios of NIST610 glass are 0.6 ± 0.6%/amu and 0.4 ± 0.5%/amu, respectively. These results, as well as the Pb-Pb age results of zircon M257 and baddeleyite Phalaborwa (see next section),

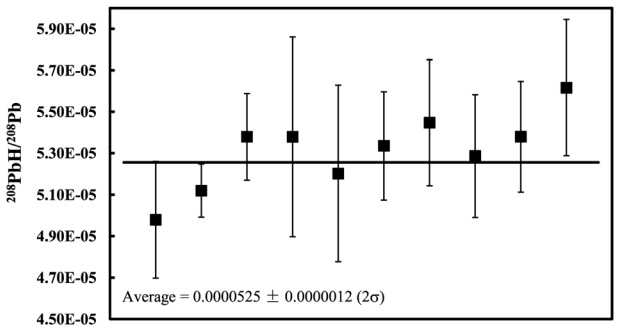

Fig. 5 $^{208}PbH/^{208}Pb$ ratios at galena (PbS) with NanoSIMS, indicating negligible hydride interference.

indicate that the IMF of Pb isotopes is negligible at mono-collector mode of NanoSIMS, confirming previous results.[11,12]

4.2. Pb-Pb age results

Pb-Pb measurements of standard zircon M257 and standard baddeleyite Phalaborwa were carried out at scanning off mode, which give a lateral resolution of <2 μm. The measured $^{204}Pb/^{206}Pb$, $^{207}Pb/^{206}Pb$ ratios and calculated $^{207}Pb^*/^{206}Pb^*$ ratios (where "*" denotes radiogenic) are summarized in Table 3. The measured $^{204}Pb/^{206}Pb$ ratios were less than 0.0001, and the common Pb of both samples is low (f_{206} <1%).

M257: Twenty-eight measurements yield a weighted average $^{207}Pb^*/^{206}Pb^*$ ratio of 0.05885 ± 0.00038 (2σ), corresponding to a Pb-Pb age of 563 ± 14 Ma (Fig. 7a). This result is consistent with the TIMS U-Pb age of 561.3 ± 0.3 Ma.[17]

Phalaborwa: Eighteen measurements give a weighted mean $^{207}Pb^*/^{206}Pb^*$ ratio of 0.12701 ± 0.00041 (2σ), corresponding to a Pb-Pb age of 2058 ± 6 Ma (Fig. 7b). This result is consistent with the best estimate age for Phalaborwa of 2059.60 ± 0.35 Ma obtained by LA-ICP-MS.[20]

4.3. U-Pb calibration

SIMS analysis exhibits significant fractionation between Pb and U, and correction of this effect is critical for precise U-Pb dating of zircon. The principle strategy for accurate correction is matrix-matched calibration by analysis of well-characterized natural zircon standards. Thus, precision and accuracy of U-Pb zircon ages highly depend on the calibration method.

Several calibration methods have been reported for the SIMS U-Pb fractionation. For example, Claoue-Long *et al.*[27] showed that the zircon Pb/U calibration curve is a Pb/U *vs.* UO/U power law with exponent 2. Sano *et al.*[11] and Takahata *et al.*[13] demonstrated that the power law relationship between Pb/UO and UO_2/UO is the best way for U-Pb calibration by using NanoSIMS. Li *et al.*[14,28] and Liu *et al.*[10] used the power law relationship between Pb/U and UO_2/U for the U-Pb calibration.

In this study, three standard zircons, including 91500, M257 and Plesovice, were selected for the calibration test. The results suggest that the power relationship between Pb/U and UO_2/U is the best fitted, and thus it is used for the U-Pb calibration here. For example, the slopes of the regression lines of the three standards for Ln(Pb/U) *vs.* Ln (UO_2/U) are similar (Fig. 8). In addition, the calculated standard deviations of slopes for Ln(Pb/U) *vs.* Ln (UO_2/U) are smaller than those of Ln(Pb/U) *vs.* Ln (UO/U) (Fig. 8). Therefore, the power law relationship between $^{206}Pb/^{238}U$ and $^{238}U^{16}O_2/^{238}U$ was utilized for U-Pb calibration in this study. The standard deviations of the Pb/U values of the reference curve were lower than 2.0%, which were accounted together with the errors from the unknowns to give an overall error for the Pb/U ratio of each analysis.

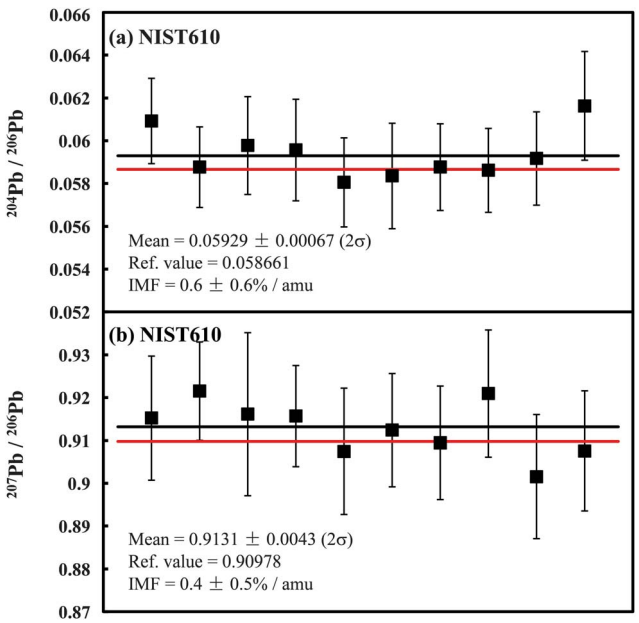

Fig. 6 Repeated measurements of $^{204}Pb/^{206}Pb$ (a) and $^{207}Pb/^{206}Pb$ ratios (b) for NIST610 glass by NanoSIMS. The instrumental mass fractionation (IMF) for Pb isotopic analysis is limited and can be negligible. Error bars are 2σ.

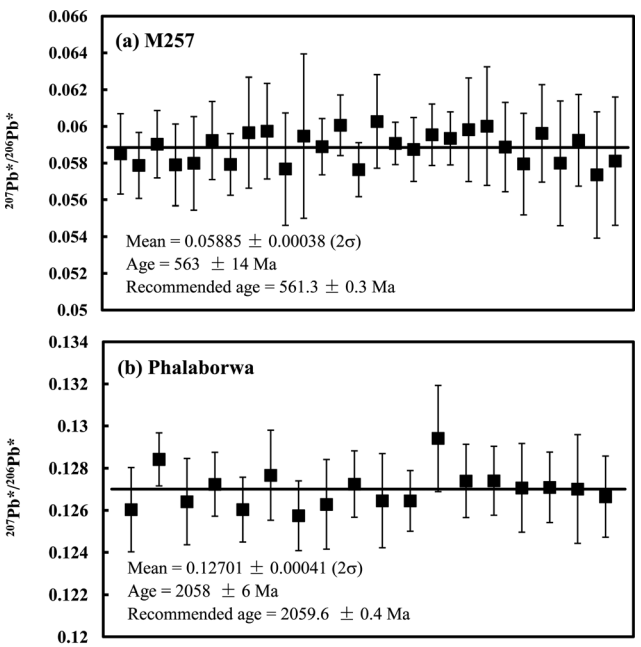

Fig. 7 Pb-Pb isotopic dating results of the standard zircon M257 (a) and standard baddeleyite Phalaborwa (b). Error bars are 2σ.

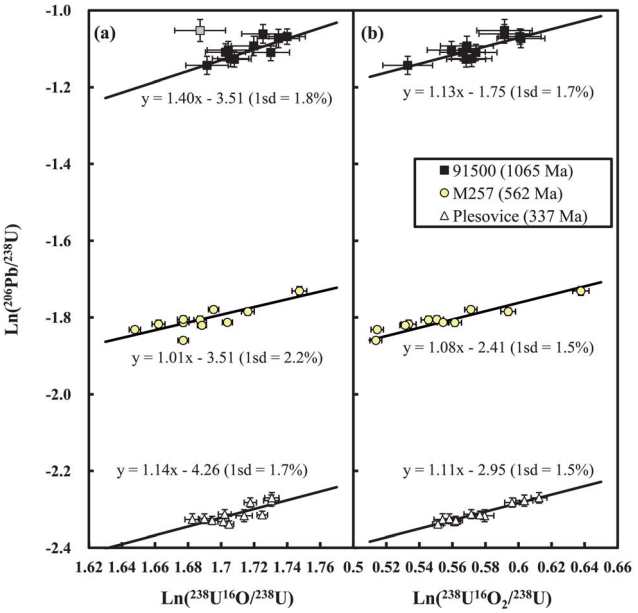

Fig. 8 Ln(^{206}Pb/^{238}U) *vs.* Ln(^{238}U^{16}O/^{238}U) (a) and Ln(^{206}Pb/^{238}U) *vs.* Ln(^{238}U^{16}O$_2$/^{238}U) (b) diagrams for standard zircons 91500, M257 and Plesovice. Error bars are 2σ.

4.4. U-Pb age results

Four standard zircons (Qinghu, Plesovice, Temora, and 91500) were measured using M257 as standard for U-Pb calibration. The results are listed in Table 4 and plotted in Fig. 9.

Qinghu: Fifteen analyses were carried out. The results are all concordant within analytical errors, yielding a weighted average ^{206}Pb/^{238}U age of 158 ± 3 Ma (Fig. 9a), which is consistent with the TIMS age of 159.5 ± 0.2 Ma.[14]

Plesovice: Seven analyses yielded a weighted average ^{206}Pb/^{238}U age of 337 ± 7 Ma (Fig. 9b), which is consistent with the ^{206}Pb/^{238}U age of 337.1 ± 0.4 Ma dated by ID-TIMS.[15]

Temora: The results of fifteen measurements analyses are all concordant within analytical errors, which gave a weighted mean ^{206}Pb/^{238}U age of 427 ± 10 Ma (Fig. 9c). This age is consistent with its ^{206}Pb/^{238}U ID-TIMS age of 416.8 ± 0.3 Ma within error.[16]

91500: The results of seven analyses are all concordant within analytical errors, yielding a weighted average ^{206}Pb/^{238}U age of 1076 ± 14 Ma (Fig. 9d), which agrees well with the ^{206}Pb/^{238}U age of 1065.4 ± 0.6 Ma by TIMS.[18]

5. Concluding remarks

Our results indicate that precise zircon and baddeleyite Pb-Pb dating at <2 μm scale and zircon U-Pb dating at <5 μm scale can be achieved using CAMECA NanoSIMS 50L. In comparison

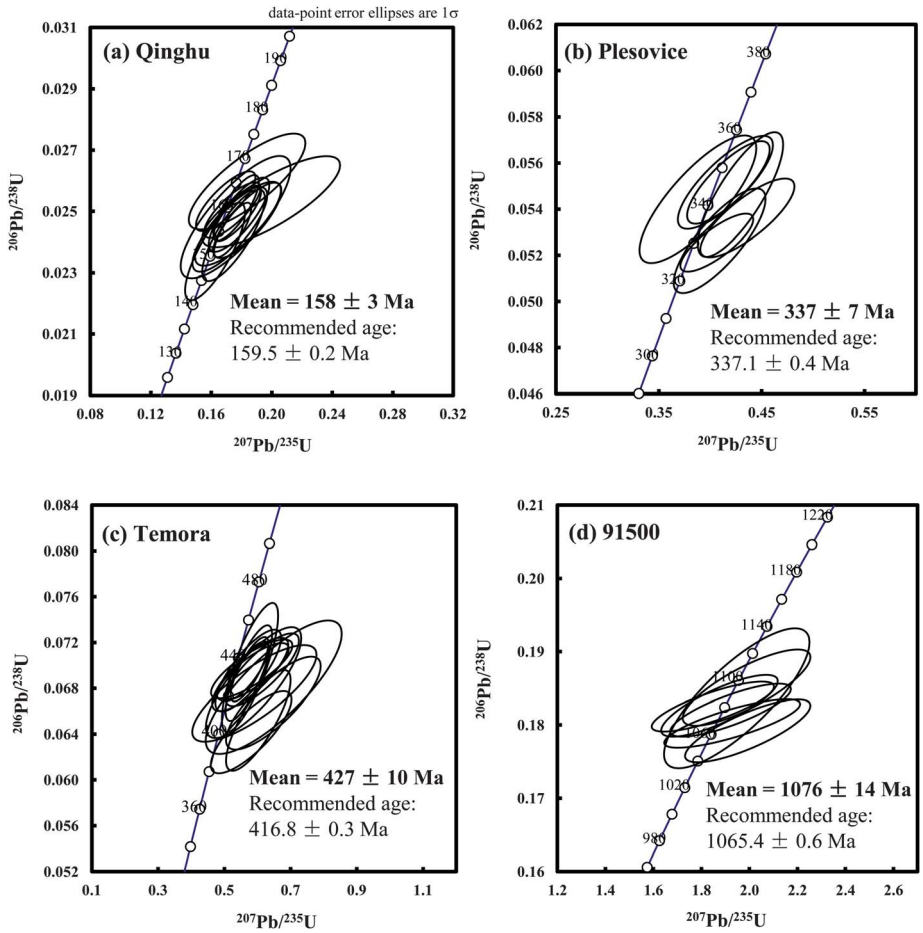

Fig. 9 U-Pb zircon Concordia diagrams for standard zircons Qinghu (a), Plesovice (b), Temora (c) and 91500 (d). Data-point error ellipses are 2σ.

with Stern *et al.*'s pilot study,[12] we optimized a higher density primary O^- ion beam of 500 pA with ~1.7 μm diameter, which is substantially brighter and smaller than that (100 pA and 4.5 μm) reported by Stern *et al*. This significantly improves the lateral resolution and precision for the Pb-Pb dating.

Takahata *et al.*[13] reported the first zircon U-Pb ages determined with NanoSIMS with the lateral resolution of 15 μm and the U-Pb age precision of about 1 ~ 2%. By doing that, we significantly improve the lateral resolution to a scale of <5 μm, with a compatible precision of 2 ~ 3%. Although NanoSIMS has the advantage of generating high current primary beam, the Pb sensitivity of NanoSIMS is significantly lower than that of CAMECA ims-1280 with oxygen flooding technique. In addition, our study demonstrates significant fractionation of U-Pb when O^- primary beam with a Gaussian illumination primary beam is used at the scanning off mode. This U-Pb fractionation can be eliminated by rastering an area of 3×3 μm^2. The U-Pb and Pb-Pb dating method demonstrated in this study will have important applications for high lateral resolution dating, such as thin layers of zoned zircons, small grains of lunar zircon, and micron-sized baddeleyites in Martian meteorites and in various achondrites from differentiated asteroids.

Acknowledgements

We thank Xianhua Li, Qiuli Li, Yu Liu, Guoqiang Tang for providing standard samples, Lu Feng, Xuchao Zhao for assistance in the lab and Fang Huang for discussions. This work was supported by the National Science Foundation of China (Grants 40803011, 41173012), the National 863 High-Tech R&D Program of China (Grant No 2009AA122201) and the Pre-planned Projects of Lunar Sample Analysis (Grant No. TY3Q20110029).

Notes and references

1 R. J. Finch and J. M. Hanchar, *Rev. Mineral. Geochem.*, 2003, **53**, 1–25.
2 D. W. Davis, T. E. Krogh and I. S. Williams, *Rev. Mineral. Geochem.*, 2003, **53**, 145–181.
3 C. A. Andersen and J. R. Hinthorne, *Earth Planet. Sci. Lett.*, 1972, **14**, 195–200.
4 W. Compston, *Journal of the Royal Society of Western Australia*, 1996, **79**, 109–117.
5 I. Williams, *Reviews in Economic Geology*, 1998, **7**, 1–35.
6 T. R. Ireland and I. S. Williams, *Rev. Mineral. Geochem.*, 2003, **53**, 215–241.
7 P. W. O. Hoskin and U. Schaltegger, *Rev. Mineral. Geochem.*, 2003, **53**, 27–62.
8 R. T. Pidgeon, A. A. Nemchin, W. van Bronswijk, T. Geisler, C. Meyer, W. Compston and I. S. Williams, *Geochim. Cosmochim. Acta*, 2007, **71**, 1370–1381.
9 A. Nemchin, N. Timms, R. Pidgeon, T. Geisler, S. Reddy and C. Meyer, *Nat. Geosci.*, 2009, **2**, 133–136.
10 Y. Liu, X.-H. Li, Q.-L. Li, G.-Q. Tang and Q.-Z. Yin, *J. Anal. At. Spectrom.*, 2011, 845–851.
11 Y. Sano, N. Takahata, Y. Tsutsumi and T. Miyamoto, *Geochem. J.*, 2006, **40**, 597–608.
12 R. A. Stern, I. R. Fletcher, B. Rasmussen, N. J. McNaughton and B. J. Griffin, *Int. J. Mass Spectrom.*, 2005, **244**, 125–134.
13 N. Takahata, Y. Tsutsumi and Y. Sano, *Gondwana Res.*, 2008, **14**, 587–596.
14 X. H. Li, Y. Liu, Q. L. Li, C. H. Guo and K. R. Chamberlain, *Geochem., Geophys., Geosyst.*, 2009, **10**, Q04010, DOI: 10.1029/2009GC002400.
15 J. Sláma, J. Kosler, D. J. Condon, J. L. Crowley, A. Gerdes, J. M. Hanchar, M. S. A. Horstwood, G. A. Morris, L. Nasdala, N. Norberg, U. Schaltegger, B. Schoene, M. N. Tubrett and M. J. Whitehouse, *Chem. Geol.*, 2008, **249**, 1–35.
16 L. P. Black, S. L. Kamo, C. M. Allen, J. N. Aleinikoff, D. W. Davis, R. J. Korsch and C. Foudoulis, *Chem. Geol.*, 2003, **200**, 155–170.
17 L. Nasdala, W. Hofmeister, N. Norberg, J. M. Martinson, F. Corfu, W. D rr, S. L. Kamo, A. K. Kennedy, A. Kronz and P. W. Reiners, *Geostand. Geoanal. Res.*, 2008, **32**, 247–265.
18 M. Wiedenbeck, P. AllÉ, F. Corfu, W. L. Griffin, M. Meier, F. Oberli, A. V. Quadt, J. C. Roddick and W. Spiegel, *Geostand. Geoanal. Res.*, 1995, **19**, 1–23.
19 L. M. Heaman and A. N. LeCheminant, *Chem. Geol.*, 1993, **110**, 95–126.
20 L. M. Heaman, *Chem. Geol.*, 2009, **261**, 43–52.
21 N. Pearce, W. Perkins, J. Westgate, M. Gorton, S. Jackson, C. Neal and S. Chenery, *Geostand. Geoanal. Res.*, 1997, **21**, 115–144.
22 J. D. Woodhead and J. M. Hergt, *Geostand. Geoanal. Res.*, 2001, **25**, 261–266.
23 F. Hillion, F. Horreard and F. Stadermann, *Proceedings of the 12th International Conference on Secondary Ion Mass Spectrometry*.
24 H. Andersen and H. Bay, in *Sputtering by Particle Bombardment I. Physical sputtering of single-element solids*., ed. R. Behrisch, Springer Berlin. 1981, vol. 47, pp. 145–218.
25 J. S. Stacey and J. D. Kramers, *Earth Planet. Sci. Lett.*, 1975, **26**, 207–221.
26 K. R. Ludwig, *Isoplot 3.0-A geochronological tookit for Microsoft Excel.*, Berkeley Geochronology Center Berkeley. 2003.
27 J. C. Claoue-Long, W. Compston, J. Roberts and C. M. Fanning, in *Geochronology, Time Scales and Global Stratigraphic Correclation*, ed. W. A. Berggren, D. V. Kent, M. P. Aubrey and J. Hardenbol. 1995, pp. 3–21.
28 Q.-L. Li, X.-H. Li, Y. Liu, G.-Q. Tang, J.-H. Yang and W.-G. Zhu, *J. Anal. At. Spectrom.*, 2010, **25**, 1107–1113.